Finite Element Modeling of Temperature Cycles in Axi-Symmetric Flash Butt Welded Thin Steel Rods and Experimental Validation

T.S. Olabamiji[1] and S.M Adedayo[2]
[1]Landmark University, Omu–Aran, Nigeria
[2]University of Ilorin, Ilorin, Nigeria
Email: olabamiji.taye@lmu.edu.ng

Abstract

Flash butt welding is a process designed to produce a forge-type butt weld between two metal pieces of similar shape. A one-dimensional finite element (FE) modeling of the temperature profile in axi–symmetric flash butt welded steel rods was carried out and results were verified by experimentation. A linear interpolation function was used in the weighted residual expression which was transformed into a matrix temperature values. Non-uniform nodal spacing was used with more concentration of nodes around the heat affected zone (HAZ). Welding process variables examined include; effect of pre-heat temperature, flash temperature, flash duration, and material geometries on temperature profile at various points along the rod. With a typical weld rod diameter of 5 mm and length 40 mm, at weld flash duration of 2 seconds peak temperatures of 572.6, 304.8, 214.2 and 170 ^{0}C were attained at distances 1, 2, 3 and 4 mm respectively from weld canter. At a distance 5 mm from weld center the thermal profile computed by finite element model were compared with experimental results obtained using type k thermocouple. Peak temperature values of 134.8 °C and 132 °C obtained for FE modeling and laboratory experiments respectively indicating a good agreement to within 2.1 % between peak temperatures.

Keywords: *Flash Butt Welding, Flash Duration, Finite Element Method, Peak Temperature, Galerkin method, Type k thermocouple*

1.0　INTRODUCTION

*R*esistance welding is a reliable, efficient and fast metal joining process with wide application in industries such as, aerospace, automobile and off-shore (Attarha and Sattari, 2011). This is due to its characteristics high speed, small heat affected zone (HAZ) and reliability in achieving a solid and consistent welding output. It is a process designed to produce a forge-type butt weld between two metal pieces of similar shape and principally used in joining ends of rods, bars, strips, rings, tubes, forgings and fittings (Sullivan and Savage, 1971). However, the non-uniformly distributed mechanical properties and residual stresses in the HAZ of a flash butt welded component may have a negative influence on the crack and fatigue life of the welded material under service and loading conditions (Jerzy, 2012; Dean and Shoichi, 2012; Ify, 2008). Thermal stress distribution arises in a body as a result of temperature gradient imposed in a body that is not free to expand in all directions (Aniy, 1993). Therefore, studies of temperature distributions as well as temperature histories are very important in understanding welding phenomenon clearly. Analytical methods are limited in their ability to clarify the physical phenomena, which take place during a typical welding operation (Li and Wang, 2013; Hwa *et al.*, 2010). With the development of computer technology and numerical analysis, simulation has become a powerful and reliable technique for the prediction of the atomic diffusion, temperature and stress fields in the welded joint (Pengkang *et al.* 2014). Although various numerical modeling techniques are available, FEM tends to be the most widely used because of its versatility (Reddy, 2006).

Numerical simulation of transient temperature in flash butt-welding using finite difference method was carried out by Adedayo and Irehovbude (2013). Allied welding processes such as friction stir welding had witnessed research works in the examination of

temperature distribution (Armin and Mehdi, 2014; Sirajuddin *et al.*, 2012; Tang *et al.*, 1998). Temperature distributions in welding with an assumption of a moving point heat source were carried out by Rosenthal (1941) and Adams (1958). Rosenthal works assumed a steady-state heat conduction relative to the moving point heat source. Mato *et al.* (2014) examined numerical and experimental residual stresses and distortions induced in T-joint welding of two plates. Within the framework of numerical investigation, a thermo-mechanical finite element analysis is performed by using a shell/three-dimensional modeling technique to improve both the computational efficiency and the accuracy. The influence of the choice of the local 3D model size on the temperature, residual stresses and displacement distributions was investigated. A minimal 3D zone size that had both appropriate convergence of the solution and accuracy was defined. Transient temperature distributions, residual stress and deformation induced by electro slag welding were obtained by Dean and Shoichi (2012). A simplified method of predicting stresses in surfaced steel rods was developed by Jerzy (2012). In his research, the dependence of stresses and strains was assumed on the basis of tension curves taking into account temperature. A study of temperature distribution in thin welded plate through experimental measurements and finite element simulation was carried out by Attarha and Sattari (2011). Boo and Cho (1990) worked on a model to obtain the transient temperature distributions in a finite thickness plate by solving a transient three-dimensional heat conduction equation with convection boundary conditions at the surface of the welding during arc welding. Hwa *et al.* (2010) examined the effect of temperature field on the sensitization of Alloy 690 welds fabricated using the gas tungsten arc welding method and the laser beam welding method. The welding thermal cycle of the two welding methods were based upon a moving heat source model.

This work develops a model temperature distribution in flash butt welding using FE solution method. Information on temperature history leads to solution prediction of thermal based mechanical properties changes and residual stresses.

2.0 METHODOLOGY

2.1 Theoretical Framework

2.1.1 Geometrical configuration
Figure 1 depicts the welding of two relatively long circular rods whose length is significantly larger than diameter. The figure also represents a schematic diagram of a one-dimensional heat flow pattern in a flash butt-welded circular rod with conductive heat moving from center towards the boundary.
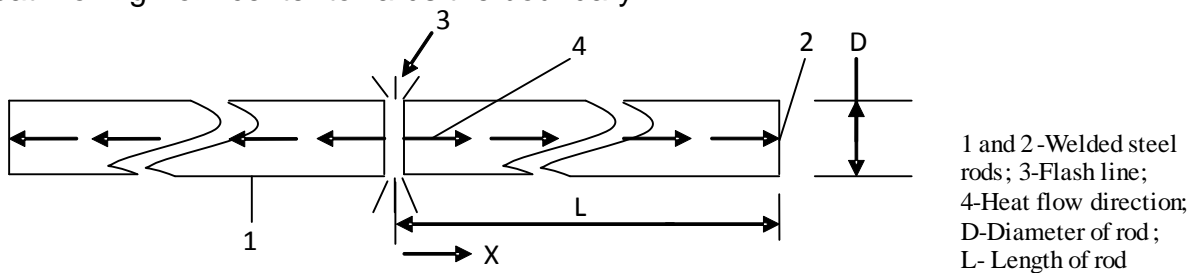
Figure 1:   Flash butt welded long rod

Upon contact of the components, a very thin layer at the interface is melted with simultaneous pressure application. Conductive heat flow is principally along the rod

length (L) while some are lost to convection and radiation at rod boundaries and circumferential surfaces.

2.1.2 Transient temperature distribution modeling
The following assumptions are made in the modeling:
(i)   Effect of applied plastic state weld pressure on temperature is assumed negligible.
(ii)   Latent heat associated with phase transformation is not factored in the temperature modeling.
(iii)   The heat transfer process is assumed to be symmetrical about the center line of the welded joint.
(iv)   Heat transfer by conduction is principally along the axial direction.
(v)   Effect of fixture and related clamping devices are neglected.
(vi)   Internal heat generation associated with metallurgical changes is assumed to be negligible.
(vii) Heat loss by convection is considered only at the circular end and circumferential curved   surfaces of the rod. (Ify, 2008; and Reddy, 2006).

Generalized governing differential equation representing temperature distribution profile in one-dimension is depicted by the partial differential parabolic equation (Reddy, 2006) as in Eq. 1.

$$\frac{\partial}{\partial x}\left(kA\frac{\partial T}{\partial x}\right) + Ag = \rho cA\frac{\partial T}{\partial t} + P\beta(T_s - T_\infty) \tag{1}$$

where: P *is the* perimeter; β *is the* convective heat transfer coefficient; T_s is the surface temperature; T_∞ is the temperature of the surrounding medium; g is the heat energy generated per unit volume; ρ *is the d*ensity; c is the specific heat capacity of the material; t is the time, k is the thermal conductivity, and A is the cross-sectional area

Application of the Galerkin's Weighted Residual Method (GWRM) to Eq. 1 and neglecting internal heat generation gives the expression in Eq. 2:

$$\sum_1^{k-1} \int_0^{h_e} N^T \left[w_e \frac{\partial T}{\partial t} + \frac{\partial}{\partial x}\left(a_e \frac{\partial T}{\partial x}\right) + (c_e T) \right] dx = 0 \tag{2}$$

where: N^T is the transpose of the shape function; h_e is the element length; $w_e = \rho.c.A$, ρ is the density of the steel the rod; c is the specific heat capacity of the material; A is the cross - sectional area of the rod

The second order term in Eq. 2 need to be reduced to the first order equivalent using integration by parts as in Eq. 3;

$$\sum_1^{k-1} \int_0^{h_e} \left[N^T w_e \frac{\partial T}{\partial t} + a_e \frac{\partial N^T}{\partial x} \frac{\partial T}{\partial x} + c_e N^T T \right] dx + \left[a_e N^T \frac{\partial T}{\partial x} \right]_0^{h_e} \tag{3}$$

Evaluation of the term $\left[a_e N^T \frac{\partial T}{\partial x} \right]_0^{h_e}$ results in Neumann's boundary condition. Its interior nodes are bound to vanish during element assembly except for the end nodes. Therefore, the term is dropped at this point because its contribution is incorporated in Neumann's boundary specification (Ify, 2008; and Reddy, 2006).

The discretized function $T(x) = [N][T]$ is substituted into Eq. 3 to yield:

$$\sum_1^{K-1} \int_0^{h_e} \left[N^T w_e \; \frac{\partial}{\partial t}([N]\{T\}) + a_e \frac{\partial N^T}{\partial x} \frac{\partial}{\partial x}([N])\{T\} + c_e \, N^T([N])\{T\} \right] dx = 0 \qquad (4)$$

The addition of the three component terms of Eq. 4 and presentation in matrix form gives:

$$\frac{\rho c A h_e}{6} \begin{bmatrix} 2 & 1 \\ 1 & 2 \end{bmatrix} \begin{Bmatrix} \dot{T_1} \\ \dot{T_2} \end{Bmatrix} + \frac{kA}{h_e} \begin{bmatrix} 1 & -1 \\ -1 & 1 \end{bmatrix} \begin{Bmatrix} T_1 \\ T_2 \end{Bmatrix} + \frac{P\beta h_e}{6} \begin{bmatrix} 2 & 1 \\ 1 & 2 \end{bmatrix} \begin{Bmatrix} T_1 \\ T_2 \end{Bmatrix} = 0 \qquad (5)$$

The assembled global matrix equation can assume the following general form as expressed in Eq. 6:

$$[A]\{\dot{T}\} + [E]\{T\} = 0 \qquad (6)$$

$[A]$ is the assemblage of the first matrix; $[E]$ is the addition of the assemblage of the second and third matrices, and $[F]$ is the assemblage flux vector.

Forward difference can be expressed as in Eq. 7,

$$\dot{T} = \frac{T^{K+1} - T^K}{\Delta t} \qquad (7)$$

Substitution of Eq. 7 into Eq. 6 yields:

$$[A]\left\{\frac{T^{K+1} - T^K}{\Delta t}\right\} + [E]\{T^K\} = 0 \qquad (8)$$

If θ is dimensionless time-weighting factor. The lownge of allowable θ values minimizes the distortion which results from the use of large time-steps in the integration of implicit difference equation. A value of θ = 0.55 minimizes distortion while conservatively ensuring theoretical stability criteria (Ify, 2008).

The introduction of dimensionless time-weighting factor, θ to Eq. 8 gives:

$$[A + \Delta t \theta E]T^{K+1} = [A - \Delta t(1 - \theta)E]\{T\}^K \qquad (9)$$

Δt is the time step; K is the time level; θ is the time-weighting factor (0.55 to 1.0 yields stable solutions). A conservative value of 0.55 produces near zero numerical dispersion (Ify, 2008), thus it is applied in this work.

2.2 Numerical Modeling and Experimental Validation

2.2.1 Finite element and computational procedure
After power activation and flash at contact surface of the rods, an interface plastic state temperature was assumed for all points located at this interface boundary.

In the numerical simulation of the flash weld, it is assumed that the two rods are welded symmetrically. The flash point is the symmetric line and thus only half of the welded rod is modeled. With the assumption of symmetry the weld line is modeled as an adiabatic boundary (Dean and Shoichi, 2012; Li and Wang, 2013; Hwa *et al.*, 2010; Pengkang *et*

al. 2014; Adedayo and Irehovbude, 2013)**.** The weldment zones are divided into a number of elements.

In the element discretization of the rod length, the specimen was divided into two parts based on element sizes (Attarha and Sattari, 2011; Li and Wang, 2013). The first portion close to weld line around the HAZ has fine and even mesh sizes while the other coarse part contains dispersed elements.

The preferred mesh size for the modeling within the refined mesh region was taken to be 0.5 mm. This was found to provide a good compromise between reasonable accuracy without excessive computation time (Attarha and Sattari, 2011; Dean and Shoichi, 2012; Li and Wang, 2013; Pengkang *et al.*, 2014; Reddy, 2006; Rosenthal, 1941; Mato *et al.*, 2014; Manole and Lage, 1993). The mesh in the remaining part was 4 mm. Linear finite element was used and mesh was chosen based on the closeness of its results with laboratory experimental values obtained as compared with other mesh sizes used in the   trial programs.

Parameters used for the numerical investigation program are: Convection coefficient = 50[W m^{-2} ^{o}C $^{-1}$], Initial temperature at weld flash line = 1,600 ^{o}C, Initial temperature at other points on rod length = 35 ^{o}C, Diameter = 5 mm, Length = 40 mm, Arc duration = 2 seconds, Number of elements = 24, Number of nodes = 25, Material type = 0.45% C Steel (k = 54 Mm^{-1} ^{o}C, c = 465 JKg^{-1} ^{o}C, ρ = 7833 kgm^{-3}). A matlab script was developed for the computational analysis.

2.2.2 Experimental procedure

Practical evaluation of the thermal history was used to verify the numerical models for correctness at point 5 mm from weld flash line. Pictorial presentation of welding arrangement is as displayed in **Figure 2** while **Figure 3** shows a schematic arrangement of temperature measurement.

A pair of 5 mm diameter by 40 mm length medium carbon steel bar was machined grooved tacked together and drilled at point 5 mm from the weld flash line. Work piece with Ni-Cr thermocouple was clamped and arc welded using ELITE BX1–250 Arc welding machine. Temperature and time readings commenced immediately the arc stabilized. The hole was tapped to an M3 size threading for thermocouple attachment. Direct temperature-time reading was taken with a Mastech digital multimeter (MY64 Series, Range: -20 ^{0}C-1000 ^{o}C, Resolution: 1 ^{o}C, Accuracy: ±(2%) and a stop watch. Arc current was 100 A, voltage – 220 V. Comparison was made with numerical model result with identical input values.
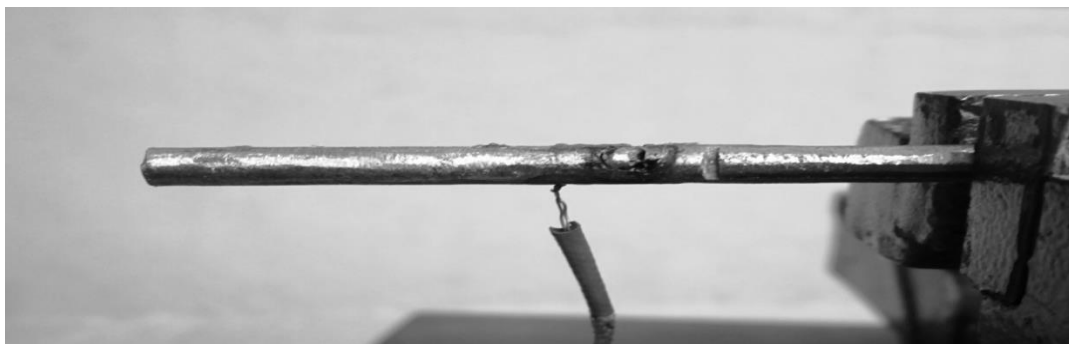

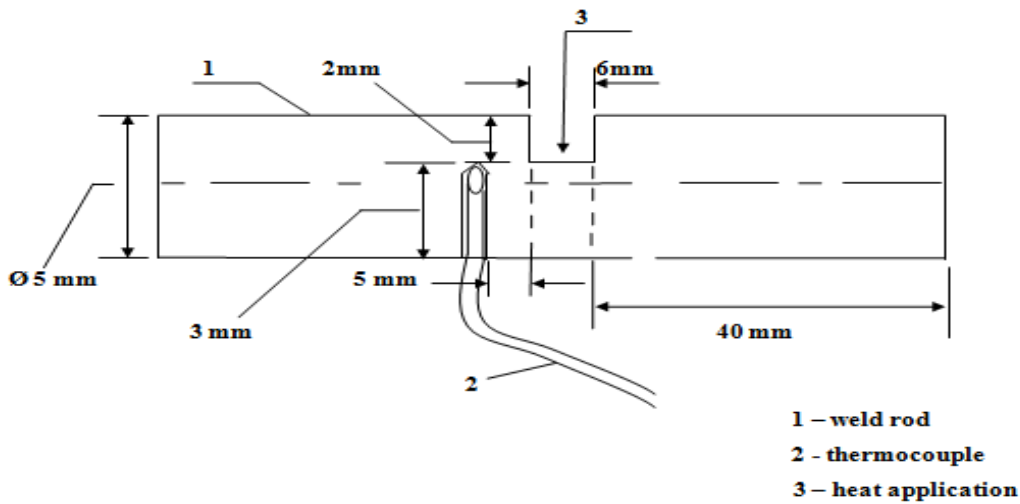**Figure 2:   Pictorial presentation of welding arrangement**

Figure 3: Schematic arrangement of temperature measurement

3.0 RESULTS AND DISCUSSION

3.1 Effect of flash point temperature on peak temperature at 1mm from flash Centre

Figure 4 represents the effect of flash point temperature on thermal history of rod at a typical point 1 mm from weld line. Flash point temperatures of 1600°C and 1800 °C resulted in peak temperatures of 572.60 °C and 641.40 °C respectively. This indicates about 12 % increase in peak temperature. Cooling was initially rapid immediately after attainment of peak temperature and subsequently slow cooling obtains. Convection accounted largely for cooling in weldments and is dependent upon the temperature differential between the material and ambient temperature. This differential is highest around peak temperature thus accounting for highest cooling rate around peak temperature.
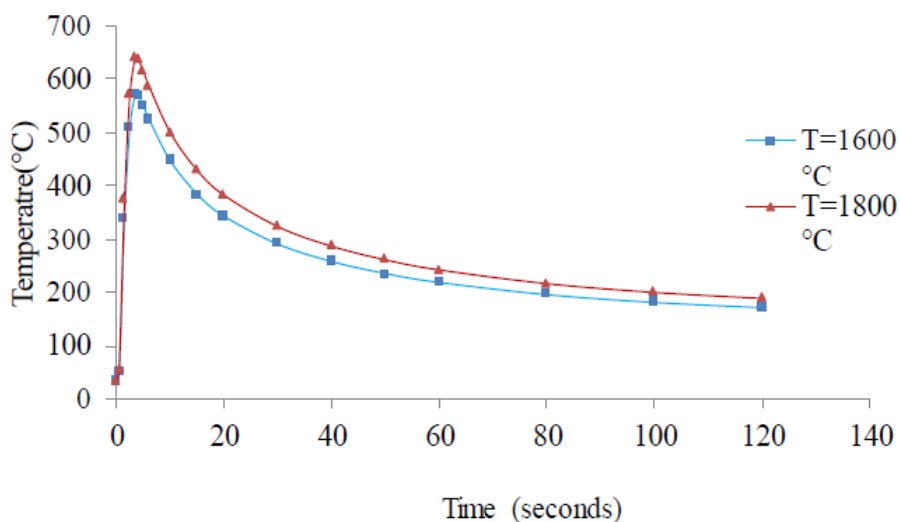

Figure 4: Temperature variation under different flash temperature at distance 1mm from weld line

3.2 Effect of distance from flash line on peak temperatures

Figure 5 displays simulated peak temperatures against distances from flash line. At distances 0.5, 1, 1.5, 2, 2.5, 3, 3.5, and 4 mm from flash line, attained peak temperatures are 971.2, 572.6, 395.32, 304.75, 250.39, 214.2, 188.4, and 169.9 °C respectively corresponding to 2.5, 3.5, 6.5, 11.5, 17.5, 24.5, 33.5 and 46.5 secs after

flash. The decrease in temperature with distance has a nonlinear trend and principally due to convective heat loss along the path of conductive heat waves in the rod.
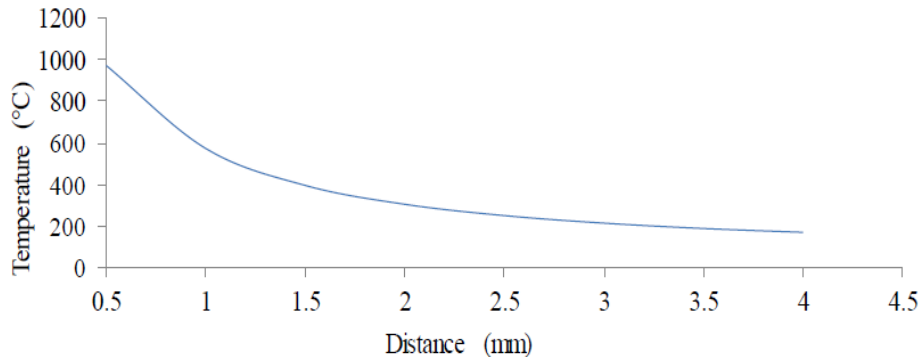

Figure 5: Variation of peak temperature with distance from weld line

3.3 Effect of distance from weld line on temperature variation
Figure 6 presents simulated thermal cycles at different distances from the weld flash line for 2 seconds flash duration. Peak temperatures of 572.6, 304.8, 214.2 and 170 ^{o}C were attained at distances 1, 2, 3 and 4 mm respectively from weld line. Time to attain peak temperatures gradually increased with distances due to time taken at such points to experience the conductive heat wave propagation. The lower peak temperature at farther distances from flash line is due to continual heat losses between the interval surfaces.
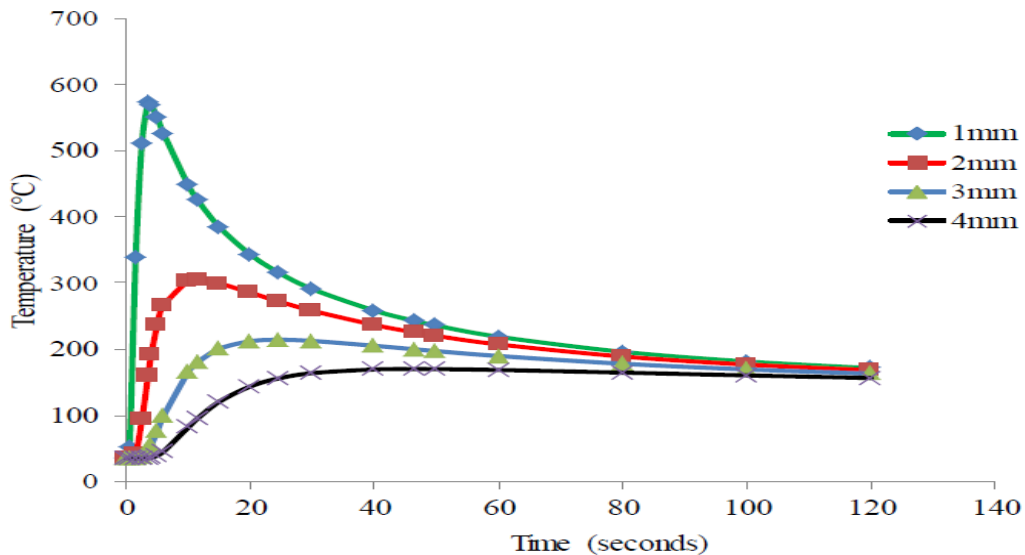

Figure 6:   Temperature variation with different distances from weld line

3.4   Effect of preheat temperature on peak temperature at distance 2 mm from the flash center: Figure 7 shows thermal history at 2 mm from weld line under metal preheat conditions. Peak temperatures of 304.8, 441.1 and 523.7 ^{o}C were attained under 35, 200 and 300 ^{o}C preheat temperatures respectively indicating 44.68 and 71.82 % increase in peak temperatures compared with nominal metal temperature of 35 ^{o}C.
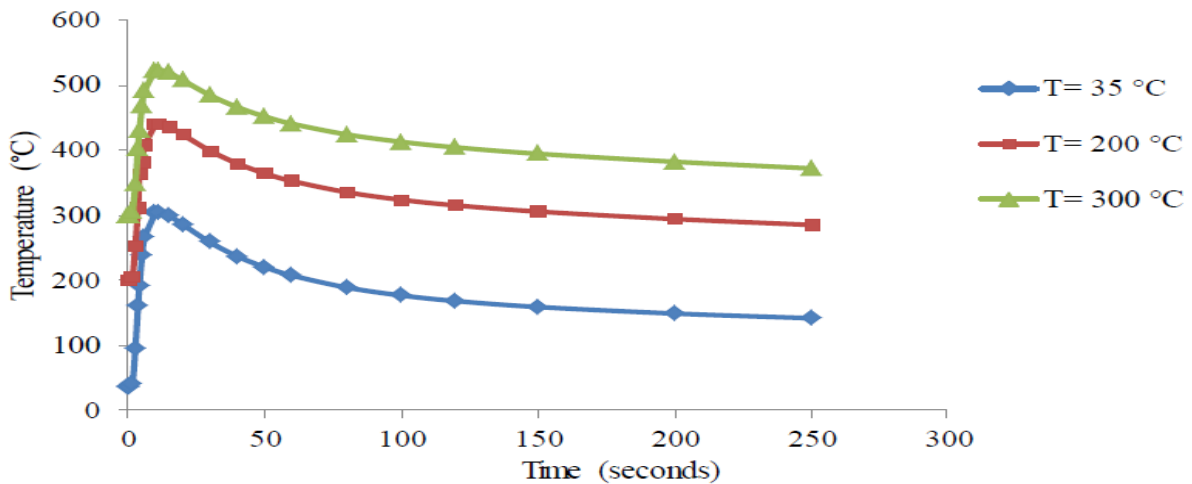
Figure 7: Thermal history under preheat at distance 3 mm from weld line

3.5 Experimental Validation of Simulated Result

The validity of simulated results is made by comparison with experimentally obtained results as shown in **Figure 8** at distance 5 mm from weld line. Simulated and experimentally obtained peak temperatures of 134.8 $^{\circ}$C and 132 $^{\circ}$C were observed, indicating a disparity of 2.1 %. This disparity is accounted for based on some heat losses not accommodated for in the simulation.
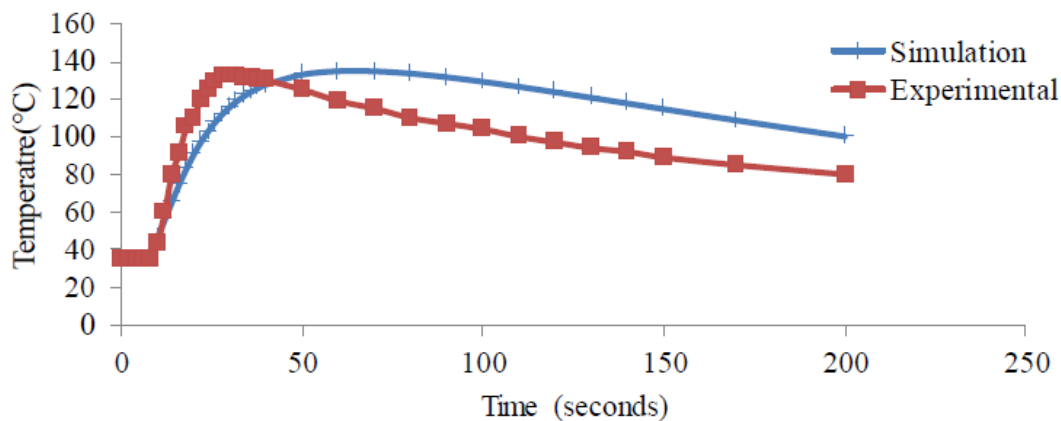

Figure 8: Numerical and experimental temperature trend at distance 5 mm from weld line

4.0 CONCLUSION

Thermal history at various points along the length of a circular section subjected to flash-butt welding was analyzed by the finite element method. From the above study the following conclusions can be drawn:

- Sharp drop in simulated temperature observed immediately after peak temperature close to the HAZ
- High peak of temperature is obtained around the heat affected zone and drops rapidly at further distances.
- Peak temperature increases with increase in flash duration and plastic temperature of metal.
- Close agreement obtains between simulation and experimental Results.

REFERENCES

Adams, J.C.M., (1958). Cooling Rates and Peak Temperatures in Fusion Welding, *Welding Journal*, 5:210 - 215.

Adedayo, S.M and Irehovbude, S.O., (2013). Numerical simulation of transient temperature in flash butt-welded axi-symmetric circular sections, *Journal of Naval Architecture and Marine Engineering*, 10:33-40.

Aniyi A. J., (1993). Effect of die and stress relief temperatures on squeeze cast aluminum alloy, Ph.D. Thesis, Department of Mechanical Engineering, University of Ilorin, Nigeria.

Armin, R and Mehdi, I., (2014). Prediction of asymmetric transient temperature and longitudinal residual stress in friction stir welding of 304L stainless steel, *Journal of Material and Design*, 55:812-820.

Attarha, M.T. and Sattari-Far I., (2011). Study on welding temperature distribution in thin welded plates through experimental measurements and finite element simulation. *Journal of Material Processing Technology*, 211: 688-694

Boo, K.S. and Cho, H.S., (1990). Transient Temperature Distribution in Arc Welding of Finite thickness plate, proceeding of the Institution of Mechanical Engineers, Part B: *Journal of Engineering Manufacture* 204:175-183.

Dean, D. and Shoichi, K., (2012). Numerical simulation of welding field, residual stress and deformation induced by electro slag welding, *Computational Material Science*, 62:23-34.

Hwa, T. L., Chun, T. C. and Jia, L.W., (2010). Numerical and experimental investigation into effect of temperature field on sensitization of Alloy 690 butt welds fabricated by gas tungsten arc welding and laser beam welding, *Journal of Material Processing Technology*, 210:1636-1645.

Ify, N. L., (2008). Finite element modeling of engineering systems, 2nd edition, University of Port Harcourt Press, Nigeria.

Jerzy, W., (2012). A simplified method of predicting stresses in surfaced steel rods, *Journal of Material Processing Technology*, 212:1080-1088.

Li, C. and Wang, Y., (2013). Three-dimensional finite element analysis of temperature and stress distributions for in-service welding process, *Material and Design*, 52:1052-1057.

Manole, D.M. and Lage, J.L., (1993). Non-uniform grid accuracy test applied to the natural-convection flow within a porous medium cavity, *Numerical Heat Transfer*, part B, 23:351-368.

Mato P., Zdenko T., Alan R., Martin S., Ivica G., Ivanka B. and Srec ′k.Š., (2014). Numerical analysis and experimental investigation of welding residual stresses and distortions in a T-joint fillet weld, *Journal of Material and Design*, 53:1052-1063.

Pengkang, Z., Li F. and Dechao, Z., (2014). Numerical simulation of transient temperature and axial deformation during linear friction welding between TC11 and TC17 titanium alloys, *Computational Material Science*, 92:325-333.

Reddy, J.N., (2006). An introduction to the finite element method, 3rd edition, Texas, Mc Graw Hill.

Rosenthal, D., (1941). Mathematical Theory of Heat Distribution during cutting and welding, *Welding Journal*, 20:220-234.

Sirajuddin, E.K., Krishnan, K.N. and Mohd, A.W., (2012). Study of Transient Temperature Distribution in a Friction Welding Process and its effects on its Joints, *International Journal of Computational Engineering Research*, 5: 1645-1655.

Sullivan, J. F. and Savage, W. F., (1971). Effect of phase control during flashing on flash weld defects, *Welding Journal*, 213-221.

Tang, W., Guo, X., McClure, J.C., Murr, L.E. and Nunes, A., (1998). Heat Input and Temperature Distribution in Friction Stir Welding, *Journal of Materials Processing and Manufacturing Science*, 7:163-172.